THE JOURNAL OF PHYSICAL CHEMISTRY B

ARTICLE

pubs.acs.org/JPCB

Dielectric Analysis of Micelles and Microemulsions Formed in a Hydrophilic Ionic Liquid. I. Interaction and Percolation

Yiwei Lian and Kongshuang Zhao*

College of Chemistry, Beijing Normal University, Beijing 100875, China

Supporting Information

ABSTRACT: Dielectric measurements were carried out on binary mixtures of Triton X-100 (TX-100, a nonionic surfactant with a polyoxyethylene chain) and 1-butyl-3-methylimidazolium tetrafluoroborate ([bmim][BF_4], a hydrophilic ionic liquid), and [bmim][BF_4]/TX-100/cyclohexane microemulsions in a wide frequency range to study the molecular interaction and percolation in these systems. Striking dielectric relaxations were observed, and the dc conductivity data were obtained from the measured total dielectric loss spectra. The interaction between TX-100 and [bmim][BF_4] is estimated by analyzing the dc conductivity of TX-100/[bmim][BF_4] solutions in light of the Bruggeman's effective medium approximation, which indicates that spherical micelles are formed when the TX-100 volume fraction is below 48% and the number of cations associated with every TX-100 molecule is eight. For IL−oil microemulsions, both the dependence of dc conductivity and the permittivity (for fixed frequency) on cyclohexane concentration were used to identify the oil-in-IL, bicontinuous, and IL-in-oil microregions. Both the conduction and dielectric relaxation behavior suggest that a static percolation occurs in this hydrophilic IL microemulsion.

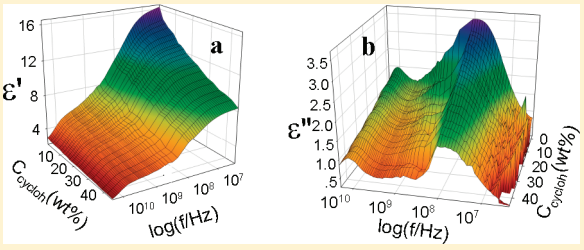

1. INTRODUCTION

Room-temperature ionic liquids (ILs) have attracted much attention as a class of solvents because of their special physical and chemical properties (such as nonflammability, low volatility, and high thermal stability) and potentially vast range of applications in chemical synthesis, industrial processing, and energy storage.[1] When the ILs serve as the solvents, the investigation for assemblies of surfactant molecule formed in ILs[2−35] is of great interest and importance. This is because these aggregations cannot only overcome the solubility limitations of ILs in immiscible solvents but also provide hydrophobic or hydrophilic nanodomains, thereby expanding the application of ILs in microheterogeneous systems as reaction, separation, and extraction media.[22] Several groups have recently prepared and characterized ILs-based micelles and microemulsions by using a variety of techniques.[2−35]

The aggregation of amphiphilic molecules into micelles is governed by the intricate balance between intermolecular interactions. de Lauth-Viguerie et al.[8] discussed the aggregation behavior of a class of nonionic surfactants in 1-butyl-3-methylimidazolium ([bmim]$^+$)-type ILs with various counterions. Armstrong et al.[4] characterized the micelles in 1-butyl-3-methylimidazolium chloride ([bmim][Cl]) and 1-butyl-3-methylimidazolium hexafluorophosphate ([bmim][PF_6]) by light scattering and small-angle neutron scattering (SANS) studies. Zheng et al.[7] studied the micelles of Triton X-100 (TX-100, a nonionic surfactant with a polyoxyethylene (PEO) chain) formed within [bmim][PF_6] and 1-butyl-3-methylimidazolium tetrafluoroborate ([bmim][BF_4]) by two-dimensional rotating frame nuclear Overhauser effect (NOE) experiments (2D ROESY) and ^{1}H NMR and found that the addition of TX-100 destroys the ion pairs of neat ILs due to the electrostatic interaction between the electronegative oxygen atoms of oxyethylene (OE) units of TX-100 and the positively charged imidazolium cations of ILs. In the study of Pandey et al.,[36] the overall data strongly indicated the partitioning of [bmim][PF_6] into the TX-100 micelle phase, which could be attributed to the interaction between [bmim]$^+$ and TX-100. However, in these previous works, the number of cations of ILs associated with TX-100, which will give quantitative understanding of the structure of ILs-based micelles, was not given.

The microemulsions with the ILs as the nanosized domains have been intensively studied.[9−35] For the preparation and characterization of microemulsions in which ILs serve as the aqueous phase, the most studied IL is [bmim][BF_4], a hydrophilic IL.[9−30] On the other hand, in the study of microemulsions in which ILs act as the oil phase, the most used IL is [bmim][PF_6], a hydrophobic IL.[32−36] In these studies, the subregions of the IL-based microemulsion, such as IL-in-oil (IL/O) or oil-in-IL (O/IL) (or IL-in-water (IL/W) or water-in-IL (W/IL)) and the transition structure between these two subregions, have been observed and divided. For example, Han et al.[9] have determined the subregions of [bmim][BF_4]/TX-100/cyclohexane microemulsions by electrical conductivity measurements and characterized the shape and size of the IL-in-oil droplets by freeze-fracturing electron microscopy (FFEM) and dynamic light scattering (DLS). In the report of Han and Li et al.,[31] the microregions of [bmim][PF_6]/TX-100/water microemulsions

Received: June 12, 2011
Revised: August 4, 2011
Published: August 22, 2011

were determined by a cyclic voltammetry method. However, the theoretical study of percolation phenomena, which can provide the dynamic picture for tracing the real micromechanism of structure transition between IL/O and O/IL (or IL/W and W/IL), is an untouched field.

In the application of micelles and microemulsions formed in ILs,[37,38] these systems may be exposed to an applied electromagnetic field. In this situation, the polarization in these systems (which appears as the permittivity) on various time scales needs to be understood; this is because these studies are helpful in investigating the distribution, diffusibility, and transition behavior of cations and anions of ILs in the interface and deciding whether the orientation of dipoles of the IL and surfactant are restricted by the interaction between them.

Dielectric relaxation spectroscopy (DRS) is a powerful method to study the physicochemical properties of micelles[39−41] and microemulsions.[42−44] Asami[41] studied the TX-100/water mixtures by DRS over wide ranges of temperatures and TX-100 concentrations and found that 2−3 water molecules hydrated with every TX-100 molecule. The dielectric experiments reported by Bhattacharya et al.[42] favored the static percolation model to describe the behavior of the permittivity. On the other hand, the dynamic percolation theory seemed to give correct results for the permittivity measurements carried out by Ponton et al.[43] and Schröle et al.[44] What's more, the broadband measured frequency range makes it so that the information involving all kinds of polarizations can be obtained at the same time by DRS.[39,40,45]

The systematic dielectric studies of neat ILs have already been reported by Weingärtner et al.,[46] Buchner et al.,[47] Nakamura et al.,[48] and so forth. The "dielectric" group of Buchner et al. has reported the dielectric analysis for the binary mixtures of ILs with dichloromethane[49] and water.[50] The work of Licence et al.[51] provided new information about the dielectric properties of ILs−water systems. In our work[52] published recently, the dielectric measurements of micelles and microemulsions formed in a hydrophobic IL were used to study the interaction, percolation, solution, and softness in these systems.

Regardless of its ability, DRS has never been applied to the micelles and microemulsions formed in hydrophilic ILs. Hence, in order to further study the interaction, percolation, and polarization in micelles and micromulsions formed in hydrophilic ILs, in this work, dielectric measurements were carried out on TX-100/[bmim][BF_4] binary mixtures and [bmim][BF_4]/TX-100/cyclohexane microemulsions. The discussion of the interaction and percolation of such systems is demonstrated in this article. The polarization, namely, the dielectric relaxation mechanisms in these systems, will be discussed in part II of this work, which will be prepared as another article.

2. EXPERIMENTAL AND METHODS

2.1. Preparation of IL-Based Micelles and Microemulsions. The IL [bmim][BF_4] (purity > 99%) was purchased from Shanghai Cheng Jie Chemical Co. Ltd., China. The residual chloride in this IL was less than 800 ppm, and the water content was less than 1000 ppm. TX-100 (p-(1,1,3,3-tetramethylbutyl)phenoxypolyoxyethyleneglycol) (reagent grade) was obtained from Amresco Chemical Inc. America. Cyclohexane was produced by Beijing Chemical Reagent Factory, China, and was analytical reagent grade. The structures of the IL and the surfactant are shown in Chart 1; they were dried under vacuum at 80 °C for 12 h to remove excess water before being used.

TX-100 was dissolved with [bmim][BF_4] at TX-100 concentration ranges from 0 to 100 wt %. The microemulsions were prepared

Chart 1. Chemical Structures of TX-100 and [bmim][BF_4]

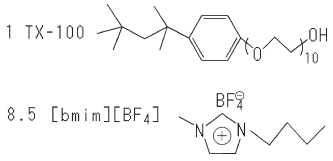

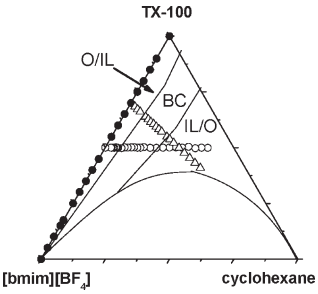

Figure 1. Experimental paths diagram of [bmim][BF_4]/TX-100/cyclohexane systems. Path ● presents the binary systems in which the weight concentration of TX-100 is from 0 (neat [bmim][BF_4]) to 100 wt % (pure TX-100); path Δ denotes the ternary systems when the weight ratio of [bmim][BF_4]/TX-100 is fixed to 3:7; and path ○ shows the ternary systems which the weight fraction of TX-100 is fixed at 50 wt %.

by mixing appropriate weight fractions of [bmim][BF_4], TX-100, and cyclohexane. The experimental paths are shown in Figure 1 (in which the boundaries are drawn according to the work of Han et al.[9]); path ● presents the TX-100/[bmim][BF_4] binary systems. Path Δ illustrates the increase of cyclohexane in microemulsions when the weight ratio of [bmim][BF_4]/TX-100 is fixed to 3:7. Path ○ demonstrates the IL-to-TX-100 molar ratio increases when the weight fraction of TX-100 in the microemulsions is fixed to 50 wt %.

2.2. Dielectric Measurements. The low-frequency dielectric measurements were performed on a 4294A precision impedance analyzer from (Agilent Technologies, made in Japan) that allows a continuous frequency measurement from 40 Hz to 110 MHz. A dielectric measurement cell with concentrically cylindrical platinum electrodes was employed[53] and connected to the impedance analyzer by a 1607E spring clip fixture (Agilent Technologies, made in Japan). The cell constant and stray capacitance were determined with air, ethanol, and pure water. The measured dielectric data were corrected by the cell constant, stray capacitance, and residual inductance according to Schwan's method.[54] The permittivity and total dielectric loss at every measured frequency were calculated from the corrected capacitance and conductance.

The high-frequency dielectric spectra were measured with an Agilent E8362B PNA series network analyzer (Agilent Technologies, made in America), equipped with an Agilent 85070E open-ended coaxial probe (Agilent Technologies, made in America), which covers the frequency ranges from 10 MHz to 20 GHz. The permittivity and total dielectric loss were automatically calculated as functions of frequency by the built-in software of this measuring system.

Both of the two measuring systems were tested and calibrated in accordance with the procedures recommended by the manufactures. The dielectric measurements for binary systems and ternary mixtures were conducted at 25 ± 0.1 and 35 ± 0.1 °C, respectively.

2.3. Data Decomposition. In an applied electric field of angular frequency ω, the dielectric properties of samples can be characterized by the complex permittivity ε^*, which is defined as

$$\varepsilon^*(\omega) = \varepsilon'(\omega) - j\frac{\kappa(\omega)}{\varepsilon_0\omega} = \varepsilon'(\omega) - j\varepsilon''(\omega) - j\frac{\kappa_l}{\varepsilon_0\omega} \quad (1)$$

where $\varepsilon'(\omega)$ is the permittivity, $j^2 = -1$, $\kappa(\omega)$ is the conductivity, ε_0 is the permittivity of vacuum, $\varepsilon''(\omega)$ is the dielectric loss, and κ_l is the low-frequency limit of conductivity (dc conductivity). $\kappa(\omega)/\varepsilon_0\omega$ is the total dielectric loss, which includes two parts, namely, the $\varepsilon''(\omega)$ and dc conductivity contribution ε''_{dc}, which can be expressed as[46−48,55]

$$\varepsilon''_{dc} = \kappa_l/\varepsilon_0\omega \quad (2)$$

The κ_l of samples in this work can be estimated according to the above equation due to the fact that ε''_{dc} cannot be neglected in the high conductivity systems. Finally, all of the dielectric loss data were obtained by subtracting the dc conductivity contribution from the total dielectric loss.

If the dielectric relaxations occur, they can be characterized by a set of dielectric parameters; ε_h is the high-frequency limit of permittivity, $\Delta\varepsilon_i$ and τ_i are the dielectric increment and the relaxation time for each mode i, respectively, and $\varepsilon_l = \Sigma\Delta\varepsilon_i + \varepsilon_h$ is the low-frequency limit of permittivity, namely, static permittivity. These dielectric parameters can be obtained by fitting the Havriliak−Negami empirical function to the experimental data[56]

$$\varepsilon^*(\omega) = \varepsilon'(\omega) - j\varepsilon''(\omega) = \varepsilon_h + \sum_i \frac{\Delta\varepsilon_i}{(1 + (j\omega\tau_i)^{\alpha_i})^{\beta_i}} \quad (3)$$

where α $(0 < \alpha \leq 1)$ and β $(0 < \beta \leq 1)$ are the parameters both related to the distribution of relaxation time and i is the number of the dielectric relaxation.

3. RESULTS AND DISCUSSION

Figure 2, as an example, shows the 3-D representations of the experimental results; (a) and (b) are the frequency dependences of permittivity and dielectric loss of [bmim][BF_4]/TX-100/cyclohexane ternary systems (when the weight ratio of IL/TX-100 is fixed as 3:7) with different cyclohexane concentrations. In Figure 2a, at least two dielectric relaxations around 0.1 and 10 GHz can be observed, which are confirmed by the two peaks of the dielectric loss spectra shown in Figure 2b. At the same time, Figure 2 obviously shows that the dielectric spectra have changed with the increasing of cyclohexane concentration.

The dc conductivity data of every measured sample were gained according to eq 2. The subtraction process of the dc conductivity contribution from the total dielectric loss of one sample is shown in Supporting Information as an example. The dc conductivities of TX-100/[bmim][BF_4] solutions are shown in Figure 4 of our previous publication.[52] The dc conductivities of [bmim][BF_4]/TX-100/cyclohexane microemulsions are shown in Figures 3 and 7 below. The dc conductivity and dielectric parameters, which reflect the electric conduction behavior and polarization properties of these systems, can provide information on the molecular interaction and dynamics of such systems from two different aspects, respectively. The interaction in IL-based micelles and the percolation in IL-based microemulsions will be discussed below.

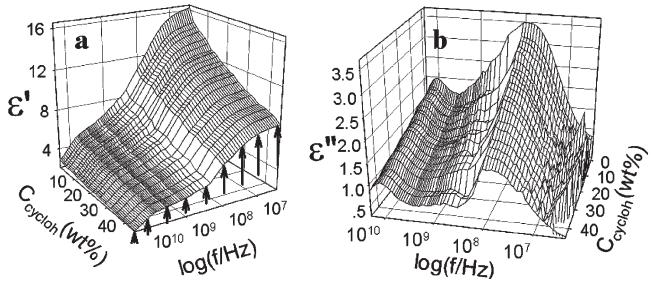

Figure 2. Three-dimensional representations for the frequency dependencies of (a) permittivity and (b) dielectric loss of [bmim][BF_4]/TX-100/cyclohexane ternary systems (when the weight ratio of IL/TX-100 is fixed as 3:7) with different cyclohexane concentrations.

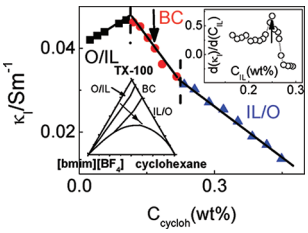

Figure 3. The dependence of the dc conductivity of [bmim][BF_4]/TX-100/cyclohexane ternary systems on cyclohexane concentration when the weight ratio of [bmim][BF_4]/TX-100 is fixed as 3:7. The data in different subregions are represented by different colored symbols. The solid lines are only to guide the eyes; the dotted lines show the probable domains of different microstructures. The lower left inset shows the composition path, where the arrow indicates the increasing direction of cyclohexane. The top right inset shows $d\kappa_l/dC_{IL}$ as a function of IL mass concentration C_{IL}, where the arrow points out the percolation threshold C_{ILp}. In the big figure, C_{ILp} is also marked by the arrow.

3.1. Interaction between TX-100 and IL. TX-100 can form micelles in [bmim][BF_4], and the cations of IL can associate with the OE units in TX-100 due to the electrostatic interaction between them.[7] In order to calculate the number of cations associated on the OE unit in [bmim][BF_4]/TX-100 solutions and understand how anions affect this association number, dielectric measurements and corresponding discussion of TX-100/[bmim][BF_4] mixtures and TX-100/[bmim][PF_6] solutions were introduced in our previous publication.[52] The main conclusions include the following. Strong interactions between ILs and TX-100 make the conductivity of [bmim][BF_4]/TX-100 mixtures decrease upon the addition of TX-100. For [bmim][BF_4]/TX-100 solutions, spherical micelles are formed when the TX-100 volume fraction is below 48% and the average number of cations associated with every TX-100 molecule is eight, which were obtained from the analysis of dc conductivity in light of the Bruggeman's effective medium approximation. Please see the detailed discussion in our previous report.[52]

3.2. Percolation in the IL−Oil Microemulsion. Percolation phenomenon, a subject of great interest, occurs along with the change of the microstructure of microemulsion. In recent years, the static[57] and dynamic[58] percolation models have been proposed for describing the mechanism of percolation. The static percolation theory contributes the percolation to the appearance of a bicontinuous (B.C.) oil and water structure,[57] while the dynamic percolation model considering the attractive interactions between water globules is responsible for the formation of

percolation clusters.[58] The transport of ions in a B.C. structure or percolation clusters gives rise to the percolation phenomenon.

These two models both show that the percolation transition takes place at a certain threshold C_p, and the relation between the conductivity and the concentration of the hydrophilic (water) phase, below and above C_p, is as follows,[42,44,57,58] respectively

$$\kappa_l \propto |C_p - C|^{-s} \quad \text{for} \quad C_p > C \tag{4}$$

$$\kappa_l \propto |C - C_p|^{\mu} \quad \text{for} \quad C_p < C \tag{5}$$

In addition, s and μ are related to a further critical exponent u through eq 6

$$u = \frac{\mu}{s + \mu} \tag{6}$$

where $\mu \approx 1.9$ both in static and dynamic theory,[61,59] $s \approx 0.7$ and $u \approx 0.73$ in static theory,[60] and $s \approx 1.2$ and $u \approx 0.61$ in dynamic theory.[61] On the other hand, DRS allows the direct determination of u via eq 7[44]

$$\varepsilon'(\omega) \approx \omega^{u-1} \tag{7}$$

In the following sections, the percolation of [bmim][BF_4]/TX-100/cyclohexane microemulsions will be discussed in terms of the percolation theories by using the conductivity and dielectric data obtained from our dielectric measurements.

3.2.1. Percolation in IL-Based Microemulsion with a Fixed Weight Ratio of [Bmim][BF_4]/TX-100. Figure 3 shows the dependence of the dc conductivity of IL−oil microemulsions on the cyclohexane concentration when the weight ratio of [bmim][BF_4]/TX-100 is fixed to 3:7. For the convenience of understanding, the figure of the experimental path is inset in Figure 3, and the arrow indicates the increase direction of cyclohexane concentration. The dc conductivity shown in Figure 3 ranges from 0.01 to 0.04 S m^{-1}, which has the same order of magnitude as the report in the literature[9] and has a more complicated dependence on cyclohexane concentration compared with the consecutive decline of the dc conductivity of binary mixtures.[52] There are two turning points in the data curve shown in Figure 3. The concentrations of these two turning points correspond to the boundaries between O/IL and B.C. and B.C. and IL/O.[9] This infers that the dc conductivity data in Figure 3 shows the concentration range of different subregions of IL microemulsion. The percolation threshold C_{ILp}(≈25.0 wt %) is obtained from the inflection point (marked by the arrows in Figure 3) of the dependence of $d\kappa_l/dC_{IL}$ on C_{IL} (shown in the top right corner of Figure 3). By using the value of C_{ILp}, the normalized distance from the percolation threshold $|(C_{IL} - C_{ILp})/C_{ILp}|$ is obtained.

As shown in Figure 3, the dc conductivity in the O/IL microemulsion increases as the cyclohexane concentration increases, which can be interpreted as the following. For the binary system, the addition of insulating TX-100 into [bmim][BF_4] can decrease the conductivity of the mixtures.[52] This is because, as concluded in section 3.1, the strong interaction between [bmim][BF_4] and TX-100 may decrease the diffusibility of the IL, which leads to the decrease of conductivity of the system. However, for the IL−oil microemulsions, the added cyclohexane can offset the conductivity reduction caused by TX-100 in two different ways. The addition of cyclohexane makes it so that (1) the TX-100 forms a surfactant film distributed between the dispersed phase and continuous phase, which results in the ILs being released from the interaction with TX-100 and participating in the electrical conduction process; this is equivalent to an increase in the conductive IL concentration; and (2) the viscosity of the system decreases, which allows easier transport of ions in the solution. That is why the conductivity of the investigated systems in the O/IL subregion increases although the IL concentration decreases. In the B.C. region, the above two effects cannot compensate for the decrease of IL concentration; thus, the dc conductivity of the system decreases. At the same time, the decline speed of the conductivity in the B.C. region is greater than that in the IL/O region due to the continuous phase of highly conductive ILs gradually transforming into the channel structure of the B.C. subregion. In the L/O subregion, although the oil is a continuous phase, because the IL has high conductivity, the dc conductivity can just continuously descend rather than reduce to a constant value at once.

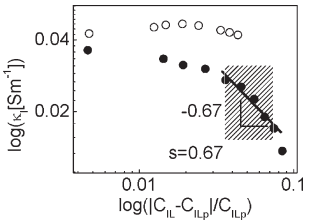

Figure 4. The scaling dependence of the dc conductivity κ_l (same as the data in Figure 3), below (full symbols) and above (open symbols) the percolation threshold C_{ILp}, on $|(C_{IL} - C_{ILp})/C_{ILp}|$. The line is the scaling fit result of the data below C_{ILp} according to eq 4.

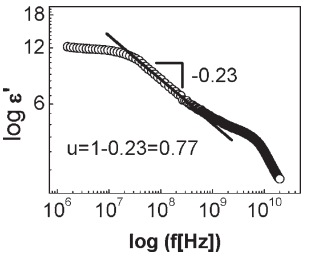

Figure 5. The frequency dependence of the permittivity of the IL−oil microemulsion at the IL concentration is 25.0 wt % (C_{ILp}) when the weight ratio of [bmim][BF_4]/TX-100 is fixed at 3:7. The straight line represents the fit to the linear part of log ε'.

The measured dc conductivity (same as the data in Figure 3) as a scaling function of $|(C_{IL} - C_{ILp})/C_{ILp}|$ is shown in Figure 4; the full and empty symbols represent the data below and above the percolation threshold, respectively. Some data (C_{IL} ranges from 17.5 to 21.4 wt %, shown in the shadow area) appear as the scaling relation with s = 0.67 (see in eq 4), represented by the solid line in Figure 4. The value of s is close to the prediction of static percolation theory.[60] The scaling behavior of the rest of the data (C_{IL} < 17.5 and >21.4 wt %) in Figure 4 cannot be described either by static or by dynamic percolation theories. These phenomena are possibly caused because the IL−oil microemulsions cannot satisfy the assumptions of the above two theories, such as the hydrophilic phase, namely, [bmim][BF_4], has high conductivity and the concentration of surfactant is too high and so forth. Although it is not enough to conclude that a static percolation occurs in this IL−oil microemulsion by the discussion of Figure 4, fortunately, the dielectric relaxation can also be used to analyze the percolation phenomena as below.

Figure 5 shows the frequency scaling of permittivity at C_{ILp} (25.0 wt %) when the weight ratio of [bmim][BF_4]/TX-100 in

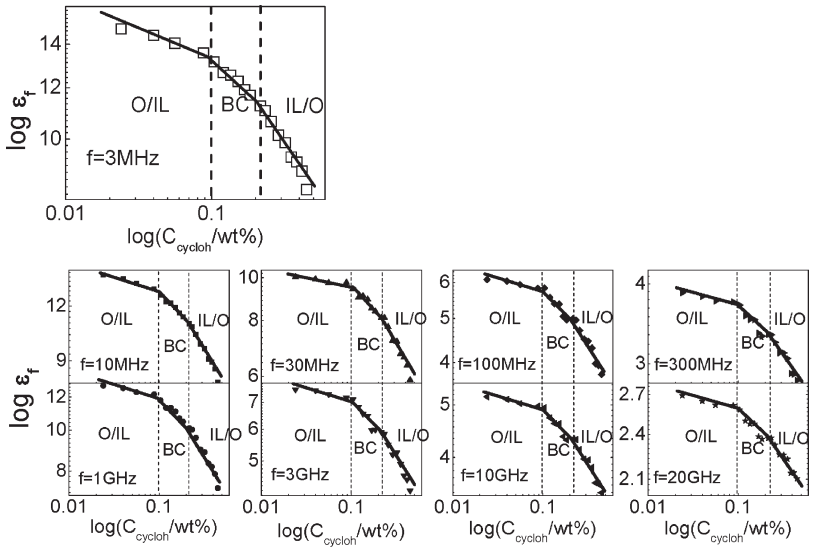

Figure 6. For the experimental path of the IL−oil microemulsion when the weight ratio of [bmim][BF_4]/TX-100 is fixed, the log−log plot of the permittivity of several selected frequencies versus the cyclohexane concentration. The selected frequencies are shown in the bottom left corner of every small figure and marked by the arrows in Figure 2a.

the IL-based microemulsion is fixed at 3:7. According to eq 7, as shown by the solid line in Figure 5, if we fit the linear part of log ε' versus log f, its slope gives $u = 0.77$. This value is close to the predicted value of the static percolation model.[60] This finding indicates that the static percolation seems to give the correct result for the permittivity measurements carried out in this work.

The value of u determined in Figure 5 is a bit greater than the prediction of static percolation theory, which can be interpreted as follows. There exists another dielectric relaxation process at a higher frequency range, which may raise the high-frequency platform of the dielectric relaxation that is used to determine u. This amounts to reduce the absolute value of the slope of the frequency scaling of permittivity, which leads to the fact that the value of u exceeds slightly the prediction of static percolation theory.

It can be seen from above discussion that due to the fact that [bmim][BF_4] has high conductivity, the three subregions in a single phase of the [bmim][BF_4]/TX-100/cyclohexane microemulsions are not as obvious as traditional microemulsions, and only part of the dc conductivity data agree with the prediction of static percolation theory. However, from the agreement between the frequency scaling of permittivity and the prediction of static percolation theory, and supported to some extent by the dc conductivity data, it can be concluded that (1) there possibly exists a bicontinuous structure in the percolation transition of this IL−oil microemulsion, and (2) a static percolation process occurs in such systems.

Both the dc conductivity and dielectric spectra suggest that the static percolation process possibly takes place in this IL−oil microemulsion. This can be explained as the 7:3 mass ratio between TX-100 and [bmim][BF_4] results in difficulty for ions to transport across the thick surfactant layer coated outside of the IL drops; only when the volume of the IL increases to a critical value and the drops touch each other to form a bicontinuous structure can the percolation process occur, caused by the transport of ions in this B.C. structure. This is similar to the concept in very concentrated suspensions and other crowded soft matter systems that jamming causes the nonequilibrium transitions from a liquid-like to a solid-like state.[62,63]

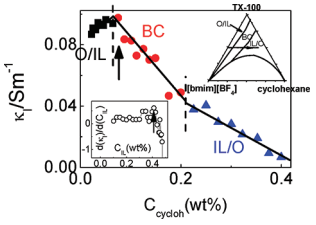

Figure 7. The dependence of the dc conductivity of the [bmim][BF_4]/TX-100/cyclohexane microemulsion on the cyclohexane concentration when the weight fraction of TX-100 is fixed at 50 wt %. Different colored symbols represent the data in different subregions. The solid lines are only to guide the eyes; the dotted lines show the probable ranges of different subregions. The top right inset shows the composition path, where the arrow indicates the increasing direction of cyclohexane. The lower left inset shows $d\kappa_l/dC_{IL}$ as a function of the IL mass concentration C_{IL}, where the arrow points out the percolation threshold C_{ILp}. In the big figure, C_{ILp} is also marked by the arrow.

Figure 6 shows the scaling dependences of permittivity of several specific frequencies on cyclohexane concentration. Two intersection points observed in Figure 6 correspond to the boundaries between O/IL and B.C. and B.C. and IL/O subregions determined by the measured dc conductivity shown in Figure 3. This finding suggests that the permittivity can also be used to determine the boundaries of the subregions of the IL−oil microemulsion.

3.2.2. Percolation in IL-Based Microemulsions with a Fixed Weight Fraction of TX-100. Figure 7 shows the dependence of the dc conductivity of the IL−oil microemulsion on cyclohexane concentration when the weight fraction of TX-100 is fixed at 50 wt %. The figure of the experimental path is inset in the top right corner of Figure 7, and the arrow indicates the direction in which the cyclohexane concentration increases. This data curve is similar to that shown in Figure 3. The two turning points shown in Figure 7 may locate the boundaries of the subregions of the IL-based microemulsion due to their concentrations being consistent with the results reported in the literature.[9] The dependence

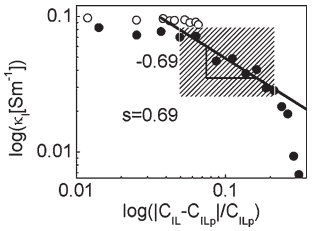

Figure 8. The scaling dependence of κ_I (the same as the data in Figure 7) on $|(C_{IL} - C_{ILp})/C_{ILp}|$; full symbols and open symbols represent the data below and above the percolation threshold C_{ILp}, respectively. The solid line is the scaling fit result of the data below C_{ILp} according to eq 4.

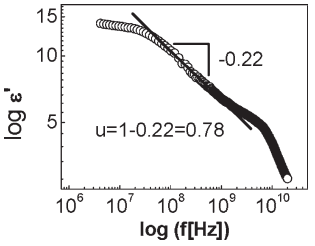

Figure 9. The frequency scaling of ε' for $C_{ILp} \approx 41.2$ wt % when the weight fraction of TX-100 in [bmim][BF_4]/TX-100/cyclohexane microemulsion is fixed at 50 wt %. The straight line represents the fit to the linear part of log ε'.

of $d\kappa_I/dC_{IL}$ on C_{IL} is also inset in the corner of Figure 7, and its inflection point gives the percolation threshold C_{ILp} (≈41.2 wt %), which is pointed out by the arrows.

Figure 8 shows the dependence of the measured dc conductivity (which is same as the data in Figure 7) on $|(C_{IL} - C_{ILp})/C_{ILp}|$; the full and empty symbols denote the data below and above the percolation threshold, respectively. The solid line in Figure 8 is the fitting result of the data (C_{IL} ranges from 20.0 to 34.9 wt %, shown in the shadow area) according to eq 4. The slope of this line is −0.69 and agrees well with the prediction of static theory,[60] which to some degree indicates that the hydrophilic IL-based microemulsions show a static percolation transition. The disagreements of other data (C_{IL} < 20.0 and >34.9 wt %) in Figure 8 with the prediction of percolation theories may be caused by the high conductivity of the IL and the interaction between the IL and surfactant again.

Figure 9 shows the frequency dependence of permittivity at C_{ILp} (41.2 wt %) when the weight fraction of TX-100 in the IL-based microemulsions is fixed at 50 wt %. The solid line in Figure 9 is the fit of the linear part of log ε' versus log f, whose slope gives $u = 0.78$. This value is again close to the prediction of the static percolation model.[60] Thus, the scaling dependence of permittivity on frequency near percolation provides a self-consistent picture of the percolation phenomenon in the IL−oil microemulsion in terms of the static percolation model. This conclusion is in good agreement with that obtained from the analysis of Figure 5. Interestingly, in the report of another series of work of ours,[52] the conduction behavior of [bmim][PF_6]/TX-100/water also indicates that a static percolation occurs in the IL−water microemulsion. That is to say that whether the IL is a hydrophilic or hydrophobic one, static percolation maybe the common feature of IL-based microemulsions.

Figure 10 shows the log−log plot of the permittivity of 10 MHz versus the cyclohexane concentration. The two

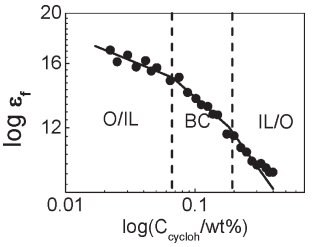

Figure 10. For the experimental path of the IL-based microemulsion when the weight fraction of TX-100 is fixed, the scaling dependence of the permittivity in 10 MHz on cyclohexane concentration.

intersection points in this data curve also correspond to the boundaries between O/IL and B.C. and B.C. and IL/O subregions determined by the dc conductivity data curve shown in Figure 7. Thus, the permittivity of fixed frequency is another method that can be used to identify the domains of the subregions of an IL-based microemulsion.

4. CONCLUSIONS

In summary, we studied, by analyzing the dc conductivity and dielectric spectra obtained from the dielectric measurements, the interaction in micelles and percolation in microemulsions formed in a hydrophilic IL, and several conclusions were reached.

For the micelles of TX-100 formed in [bmim][BF_4], the micelles present a spherical shape when the TX-100 volume fraction is below 48%; The number of imidazolium cations associated with every TX-100 molecule is eight. This value is less than the number of waters hydrated on each TX-100 molecule and the association number of cations per TX-100 molecule in TX-100/[bmim][PF_6] mixtures, which reflects the influence of the cationic and anionic volume effects on the structure of IL-based micelles, respectively.

For two experimental paths that both lie across the three different subregions of [bmim][BF_4]/TX-100/cyclohexane microemulsion, the concentration ranges of the oil-in-IL, B.C., and IL-in-oil microregions of IL-based microemulsions were identified by the dependence of dc conductivity and permittivity (of fixed frequency) as a function of the cyclohexane concentration at the same time. Furthermore, not only the scaling dependence of the dc conductivity on the cyclohexane concentration but also the scaling dependence of permittivity on frequency near the percolation transition suggest that a static percolation occurs in this IL−oil microemulsion. The frequent appearances of scaling dependencies in this paper could be one of the common features of soft matter and reflect the existence of mesoscopic ordered structures of IL-based microemulsions.

■ ASSOCIATED CONTENT

Supporting Information. The subtraction process of the dc conductivity contribution from the total dielectric loss. This material is available free of charge via the Internet at http://pubs.acs.org.

■ AUTHOR INFORMATION

Corresponding Author

*E-mail: zhaoks@bnu.edu.cn. Tel: +861058808283. Fax: +861058802075.

■ ACKNOWLEDGMENT

The authors wish to thank Jinmei Pan and Shaojie Zhao for helpful measurement of high-frequency data. Financial support of this work by the National Natural Science Foundation of China (No. 21173025, 20976015) is gratefully acknowledged.

■ REFERENCES

(1) Wasserscheid, P., Welton, T., Eds. *Ionic Liquids in Synthesis*; Wiley-VCH: Weinheim, Germany, 2003.
(2) Merrigan, T. L.; Bates, E. D.; Dorman, S. C.; Davis, J. H. *Chem. Commun.* **2000**, 2051–2052.
(3) Headley, A. D.; Jackson, N. M. *J. Phys. Org. Chem.* **2002**, *15*, 52–55.
(4) Anderson, J. L.; Pino, V.; Hagberg, E. C.; Sheares, V. V.; Armstrong, D. W. *Chem. Commun.* **2003**, 2444–2445.
(5) Fletcher, K. A.; Pandey, S. *Langmuir* **2004**, *20*, 33–36.
(6) Seth, D.; Chakraborty, A.; Setua, P.; Sarkar, N. *J. Phys. Chem. B* **2007**, *111*, 4781–4787.
(7) Gao, Y. A.; Li, N.; Li, X. W.; Zhang, S. H.; Zheng, L. Q.; Bai, X. T.; Yu, L. *J. Phys. Chem. B* **2009**, *113*, 123–130.
(8) Patrascu, C.; Gauffre, F.; Nallet, F.; Bordes, R.; Oberdisse, J.; de Lauth-Viguerie, N. *ChemPhysChem* **2006**, *7*, 99–101.
(9) Gao, H. X.; Li, J. C.; Han, B. X.; Chen, W. N.; Zhang, J. L.; Zhang, R.; Yan, D. D. *Phys. Chem. Chem. Phys.* **2004**, *6*, 2914–2916.
(10) Li, J.; Zhang, J.; Han, B.; Wang, Y.; Gao, L. *J. Chem. Phys.* **2004**, *121*, 7408–7412.
(11) Liu, J.; Cheng, S.; Zhang, J.; Feng, X.; Fu, X.; Han, B. *Angew. Chem.* **2007**, *119*, 3377–3379.
(12) Gao, Y.; Wang, S.; Zheng, L.; Han, S.; Zhang, X.; Lu, D.; Yu, L.; Ji, Y.; Zhang, G. *J. Colloid Interface Sci.* **2006**, *301*, 612–616.
(13) Gao, Y.; Zhang, J.; Xu, H.; Zhao, X.; Zheng, L.; Li, X.; Yu, L. *ChemPhysChem* **2006**, *7*, 1554–1561.
(14) Li, N.; Gao, Y. A.; Zheng, L. Q.; Zhang, J.; Yu, L.; Li, X. W. *Langmuir* **2007**, *23*, 1091–1097.
(15) Gao, Y.; Li, N.; Zheng, L.; Zhao, X.; Zhang, J.; Cao, Q.; Zhao, M.; Li, Z.; Zhang, G. *Chem.—Eur. J.* **2007**, *13*, 2661–2670.
(16) Li, N.; Cao, Q.; Gao, Y.; Zhang, J.; Zheng, L.; Bai, X.; Dong, B.; Li, Z.; Zhao, M.; Yu, L. *ChemPhysChem* **2007**, *8*, 2211–2217.
(17) Gao, Y.; Li, N.; Zheng, L.; Bai, X.; Yu, L.; Zhao, X.; Zhang, J.; Zhao, M.; Li, Z. *J. Phys. Chem. B* **2007**, *111*, 2506–2513.
(18) Li, N.; Zhang, S. H.; Zheng, L. Q.; Gao, Y. A.; Yu, L. *Langmuir* **2008**, *24*, 2973–2976.
(19) Li, N.; Zhang, S.; Zheng, L.; Gao, Y.; Yu, L. *Colloid Polym. Sci.* **2009**, *287*, 103–108.
(20) Gao, Y.; Li, N.; Hilfert, L.; Zhang, S.; Zheng, L.; Yu, L. *Langmuir* **2009**, *25*, 1360–1365.
(21) Gao, Y.; Li, N.; Zhang, S.; Zheng, L.; Li, X.; Dong, B.; Yu, L. *J. Phys. Chem. B* **2009**, *113*, 1389–1395.
(22) Eastoe, J.; Gold, S.; Rogers, S. E.; Paul, A.; Welton, T.; Heenan, R. K.; Grillo, I. *J. Am. Chem. Soc.* **2005**, *127*, 7302–7303.
(23) Chakrabarty, D.; Seth, D.; Chakraborty, A.; Sarkar, N. *J. Phys. Chem. B* **2005**, *109*, 5753–5758.
(24) Gao, Y.; Voigt, A.; Hilfert, L.; Sundmacher, K. *ChemPhysChem* **2008**, *9*, 1603–1609.
(25) Adhikari, A.; Sahu, K.; Dey, S.; Ghosh, S.; Mandal, U.; Bhattacharyya, K. *J. Phys. Chem. B* **2007**, *111*, 12809–12816.
(26) Adhikari, A.; Das, D. K.; Sasmal, D. K.; Bhattacharyya, K. *J. Phys. Chem. A* **2009**, *113*, 3737–3743.
(27) Gao, Y.; Hilfert, L.; Voigt, A.; Sundmacher, K. *J. Phys. Chem. B* **2008**, *112*, 3711–3719.
(28) Gao, Y.; Voigt, A.; Hilfert, L.; Sundmacher, K. *Colloid Surf. A* **2008**, *329*, 146–152.
(29) Cheng, S.; Han, F.; Wang, Y.; Yan, J. *Colloid Surf. A* **2008**, *317*, 457–461.
(30) Atkin, R.; Warr, G. G. *J. Phys. Chem. B* **2007**, *111*, 9309–9316.
(31) Gao, Y. A.; Han, S. B.; Han, B. X.; Li, G. Z.; Shen, D.; Li, Z. H.; Du, J. M.; Hou, W. G.; Zhang, G. Y. *Langmuir* **2005**, *21*, 5681–5684.
(32) Seth, D.; Chakraborty, A.; Setua, P.; Sarkar, N. *Langmuir* **2006**, *22*, 7768–7775.
(33) Seth, D.; Chakraborty, A.; Setua, P.; Sarkar, N. *J. Chem. Phys.* **2007**, *126*, 224512.
(34) Gao, Y.; Li, N.; Zheng, L.; Zhao, X.; Zhang, S.; Han, B.; Hou, W.; Lia, G. *Green Chem.* **2006**, *8*, 43–46.
(35) Anjum, N.; Guedeau-Boudeville, M.-A.; Stubenrauch, C.; Mourchid, A. *J. Phys. Chem. B* **2009**, *113*, 239–244.
(36) Behera, K.; Dahiya, P.; Pandey, S. *J. Colloid Interface Sci.* **2007**, *307*, 235–245.
(37) Dong, B.; Zhang, S.; Zheng, L.; Xu, J. *J. Electroanal. Chem.* **2008**, *619−620*, 193–196.
(38) Dong, B.; Xu, J.; Zheng, L.; Hou, J. *J. Electroanal. Chem.* **2009**, *628*, 60–66.
(39) Baar, C.; Buchner, R.; Kunz, W. *J. Phys. Chem. B* **2001**, *105*, 2906–2913.
(40) Baar, C.; Buchner, R.; Kunz, W. *J. Phys. Chem. B* **2001**, *105*, 2914–2922.
(41) Asami, K. *J. Phys.: Condens. Matter* **2007**, *19*, 376102.
(42) Bhattacharya, S.; Stokes, J. P.; Kim, M. W.; Huang, J. S. *Phys. Rev. Lett.* **1985**, *55*, 1884–1887.
(43) Ponton, A.; Bose, T. K.; Delbos, G. *J. Chem. Phys.* **1991**, *94*, 6879–6886.
(44) Schröle, S.; Buchner, R.; Kunz, W. *ChemPhysChem* **2005**, *6*, 1051–1055.
(45) Kremer, F.; Schönhals, A. *Broadband Dielectric Spectroscopy*; Springer: Berlin, Germany, 2003.
(46) Daguenet, C; Dyson, P. J.; Krossing, I.; Oleinikova, A.; Slattery, J.; Wakai, C.; Weingärtner, H. *J. Phys. Chem. B* **2006**, *110*, 12682–12688.
(47) Stoppa, A.; Hunger, J.; Buchner, R.; Hefter, G.; Thoman, A.; Helm, H. *J. Phys. Chem. B* **2008**, *112*, 4854–4858.
(48) Nakamura, K.; Shikata, T. *ChemPhysChem* **2010**, *11*, 285–294.
(49) Hunger, J.; Stoppa, A.; Buchner, R.; Hefter, G. *J. Phys. Chem. B* **2008**, *112*, 12913–12919.
(50) Schröder, C.; Hunger, J.; Stoppa, A.; Buchner, R.; Steinhauser, O. *J. Chem. Phys.* **2008**, *129*, 184501.
(51) Dimitrakis, G.; Villar-Garcia, I. J.; Lester, E.; Licence, P.; Kingman, S. *Phys. Chem. Chem. Phys.* **2008**, *10*, 2947–2951.
(52) Lian, Y.; Zhao, K. *Soft Matter* **2011**, DOI: 10.1039/C1SM05491K.
(53) Hanai, T.; Zhang, H.-Z.; Sekine, K.; Asaka, K.; Asami, K. *Ferroelectrics* **1988**, *86*, 191–204.
(54) Schwan, H. P. Determination of Biological Impedance. In *Physical Techniques in Biological Research*; Nastuk, W. L., Ed.; Academic PressL New York and London, 1963; p 323.
(55) Mitsumata, T.; Gong, J. P.; Ikeda, K.; Osada, Y. *J. Phys. Chem. B* **1998**, *102*, 5246–5251.
(56) Cole, K. S.; Cole, R. H. *J. Chem. Phys.* **1941**, *9*, 341–351.
(57) Talmon, Y.; Prager, S. *J. Chem. Phys.* **1978**, *69*, 2984–2991.
(58) Laguës, M. *J. Phys. (Paris)* **1979**, *40*, L331.
(59) Derrida, B.; Stauffer, D.; Hermann, H. J.; Vannimenus, J. *J. Phys. (Paris)* **1983**, *44*, L701.
(60) de Gennes, P. G. *J. Phys. (Paris)* **1980**, *41*, C3–17.
(61) Grest, G. S.; Webman, I.; Safran, S. A.; Bug, A. L. *Phys. Rev. A* **1986**, *33*, 2842–2845.
(62) Liu, A. S.; Nagel, R. *Nature (London)* **1998**, *396*, 21–22.
(63) Trappe, V.; Prasad, V.; Cipelletti, L.; Segre, P. N.; Weitz, D. A. *Nature (London)* **2001**, *411*, 772–775.